

Many-body Bell's inequalities from average two-body correlations

Guillem Müller-Rigat,¹ Albert Aloy,¹ Maciej Lewenstein,^{1,2} and Irénée Frerot^{1,3,*}

¹*ICFO - Institut de Ciències Fotoniques, The Barcelona Institute of Science and Technology, 08860 Castelldefels (Barcelona), Spain*

²*ICREA, Pg. Lluís Companys 23, 08010 Barcelona, Spain*

³*Max-Planck-Institut für Quantenoptik, D-85748 Garching, Germany*

(Dated: June 16, 2022)

Violating Bell's inequalities allows one to certify the preparation of entangled states from minimal assumptions – in a device-independent manner. Finding Bell's inequalities tailored to many-body correlations as prepared in present-day quantum simulators is however a highly challenging endeavour. Here, we develop a novel data-driven approach to find Bell's inequalities violated by very coarse-grain features of the system: two-body correlations averaged over all permutations of the subsystems. This very flexible method, whose complexity does not scale with the system size, allows us to systematically improve over the previously known Bell's inequalities robustly violated by ensembles of quantum spins $j = 1/2$; and to discover novel families of Bell's inequalities, tailored to spin-squeezed states and many-body spin singlets of arbitrary spins ($j > 1/2$).

PACS numbers:

I. INTRODUCTION

Multipartite entanglement is a central feature of quantum many-body systems, fundamentally challenging our ability to efficiently simulate them on classical computers [1, 2]. For the same reason, quantum entanglement distributed among many degrees of freedom represents a key resource for quantum simulators and computers. Consequently, proving that the multipartite states prepared in quantum simulators or computers are indeed entangled – namely, the task of entanglement certification – is a key step in assessing the quantum advantage offered by such devices. Depending on the assumptions made about the individual components of the device, two different paradigms may appear suitable. In a so-called device-dependent framework, the subsystems are well characterized: the Hilbert space is known (e.g. a qubit space), and the measurements correspond to well-defined quantum observables (e.g. spin measurements); in this framework, entanglement certification relies on the violation of a certain entanglement witness [3]. On the other hand, in a device-independent framework, no assumption is made about the Hilbert space of the subsystems, and consequently the measurements correspond to unknown quantum observables; this framework appears especially suitable when considering effective few-level systems such as superconducting qubits. Relaxing certain assumptions about the system clearly makes entanglement certification more demanding; nevertheless, device-independent entanglement certification is possible if the violation of a certain Bell's inequality [4] can be established.

As fully characterizing the many-body correlations

among the subsystems requires exponentially-many measurements [5], any scalable method must rely on incomplete information, obtained from an accessible number of measurements – for instance, the knowledge of few-body correlations among the subsystems [6–9], or the knowledge of a few global properties [10]. A second challenge for entanglement certification is to take advantage, to the largest possible extent, of all the available information, without *a priori* knowing the structure of entanglement within the many-body state. In particular, failing to pass all existing entanglement tests criteria does not imply that entanglement certification is impossible based on available data. This motivates the development of *data-driven* methods [8, 9, 11], where the data serve as input into an algorithm which builds, from the data themselves, a tailored entanglement criterion. A successful strategy to mitigate or avoid scalability issues is often to symmetrize the data from which entanglement is to be certified. On the experimental level [7, 12], this allows to reduce the number of independent measurements to implement, and to lower the imprecision on the data themselves. On the theoretical side, this allows to reduce the computational complexity of the entanglement certification methods [6, 9–11, 13], sometimes leading to analytical characterization of the entanglement criteria [6, 10].

Here, we focus on a device-independent scenario for entanglement certification. We develop a very efficient and flexible data-driven method which takes, as input data, one- and two-body correlation functions averaged over all permutations of the subsystems. Considering only such coarse-grained features of the correlations – depending only on zero-momentum fluctuations –, we are able to circumvent all scalability issues, and devise a convex-optimization algorithm whose complexity is independent of the system size, which reconstructs a Bell's inequality violated by the data. As first results obtained

*ireneefrerot@icfo.eu

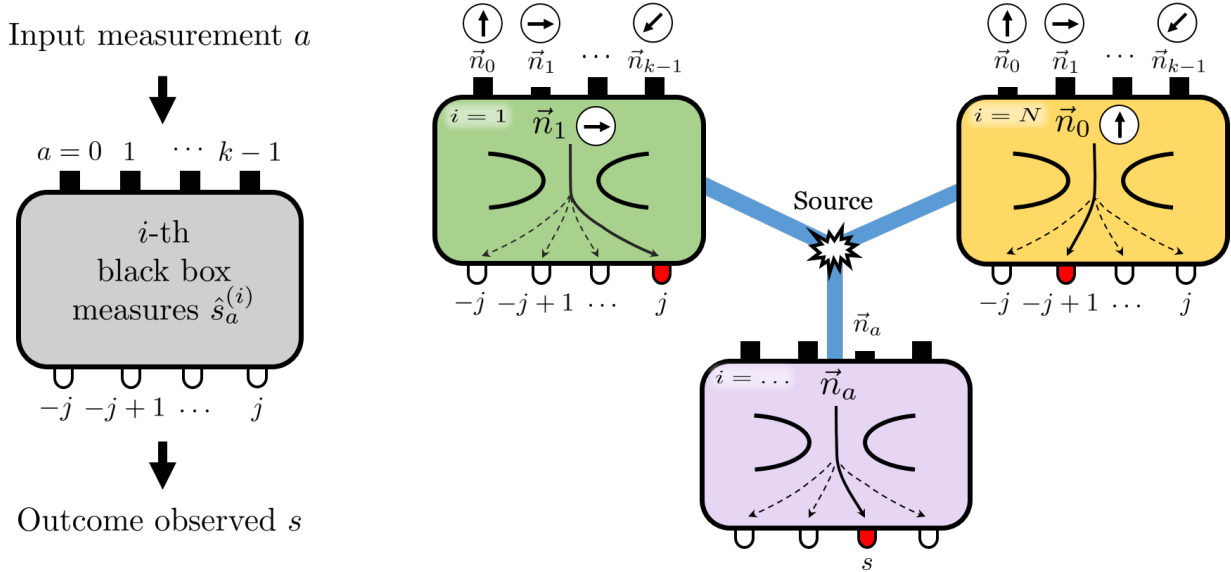


FIG. 1: Illustration of an ideal multipartite Bell test for entanglement certification. Right: A composite quantum system prepared by the source is shared among N spatially-separated observers (on the sketch, $N = 3$), each of which chooses a measurement settings $a \in \{0, 1, \dots, k - 1\}$, obtaining an outcome $s \in \{-j, -j + 1, \dots, j\}$. In this work, we focus on spin measurements on quantum spin- j particles, sketched as Stern-Gerlach magnets oriented along directions \vec{n}_a – but Bell tests are independent of these assumptions. This procedure is repeated several times in order to accumulate statistics, where at each round the measurement settings and the observed outcomes may vary. If the observed statistics exhibit Bell’s non-local correlations, one certifies that the multipartite state is quantum-mechanically entangled. Left: In a Bell test, each subsystem i is treated as a black box, with no assumption about the Hilbert space. The actual observables $\hat{s}_a^{(i)}$ being measured are attributed arbitrary input labels a , and the measurement outcomes s have no physical meaning. Entanglement is therefore certified in a device-independent manner.

with this novel method for device-independent entanglement certification, we discover new many-body Bell’s inequalities, for measurements involving arbitrarily-many outcomes, violated by paradigmatic many-body entangled states for ensembles of quantum spins $j \geq 1/2$ – namely, spin singlets and spin-squeezed states. Before entering into the details of our new method, we review the framework of device-independent entanglement certification, and the notion of Bell’s inequalities invariant under permutations.

A. Device-independent entanglement certification

Bell scenario. Arguably, the violation of Bell’s inequalities [4] represents the most robust scheme to certify entanglement, avoiding detailed assumptions about the physical nature of the degrees of freedom being measured, and about the accurate calibration of the measurements being performed. In this so-called device-independent scenario (Fig. 1), each subsystem $i \in \{1, \dots, N\}$ (for instance, a quantum spin- j) is treated as a black box, namely, no assumption is made about the actual Hilbert space of the system. This black-box treatment is especially relevant when dealing with effective few-level systems. On each subsystem, k different measurement settings can be implemented. In practice, they correspond

to certain quantum operators $\hat{s}_a^{(i)}$ ($a \in \{0, \dots, k - 1\}$), for instance spin measurements along particular directions \mathbf{n}_a , but in a device-independent scenario the actual quantum measurement which is performed is not assumed; instead, only the outcome of the measurement, denoted s , is collected (see Fig. 1). The only assumption made is that the number d of possible outcomes for each measurement is finite. In practice, the possible values of s are the eigenvalues of the quantum operator $\hat{s}_a^{(i)}$ (for instance, the $2j + 1$ possible values of a spin- j measurement), but in a device-independent scenario these are mere labels for the outcomes, with no specific physical meaning. For convenience and later connection with quantum violations of Bell’s inequalities when performing appropriate spin measurements on quantum many-body systems, we denote these possible outcomes as $s \in \{-j, -j + 1, \dots, j\}$ with $d = 2j + 1$ – but it should be emphasized that within a device-independent framework, these labels are arbitrary. A Bell experiment [4] consists in repeating the following sequence: 1) choose a setting $a^{(i)} \in \{0, \dots, k - 1\}$ for each subsystem; 2) perform the corresponding measurements, yielding the N outcomes $\mathbf{s} = \{s^{(i)}\}_{i=1}^N$. By repeating this sequence, varying the measurement settings $\mathbf{a} = \{a^{(i)}\}_{i=1}^N$, statistics of the measurement outcomes are collected. Complete information is obtained if one reconstructs all N -body marginal probability distributions: $P(\mathbf{s}|\mathbf{a})$ for all choices of settings \mathbf{a} . If one

denotes $\hat{\Pi}_{a,s}^{(i)}$ the projector onto the eigenspace of the observable $\hat{s}_a^{(i)}$ associated to the eigenvalue s , then these probabilities are given by

$$P(\mathbf{s}|\mathbf{a}) = \text{Tr}[\rho \otimes_{i=1}^N \hat{\Pi}_{a^{(i)},s^{(i)}}^{(i)}], \quad (1)$$

where ρ is the density-matrix of the system – notice that even if, in a device-independent scenario, we remain agnostic about the Hilbert space over which ρ acts, such a decomposition exists in principle.

Bell's inequalities and entanglement certification. The state ρ is not entangled (namely, it is separable) if it can be decomposed as a statistical mixture of product states:

$$\rho_{\text{sep}} = \int_{\lambda} d\mu(\lambda) \otimes_{i=1}^N \rho_{\lambda}^{(i)}, \quad (2)$$

where $\rho_{\lambda}^{(i)}$ is an arbitrary local quantum state (pure or mixed) for subsystem i , acting on the local Hilbert space whose dimension is arbitrary. λ is some classical random variable, sampled with probability measure $d\mu(\lambda)$, which encodes classical correlations among the local quantum states $\rho_{\lambda}^{(i)}$. The central observation behind device-independent entanglement certification is that if ρ is separable [Eq. (2)], then $P(\mathbf{s}|\mathbf{a})$ can always be reproduced by a local-variable (LV) model in the sense of J. S. Bell [4, 14]:

$$P_{\text{LV}}(\mathbf{s}|\mathbf{a}) = \int_{\lambda} d\mu(\lambda) \prod_{i=1}^N P_{\lambda}^{(i)}[s^{(i)}|a^{(i)}], \quad (3)$$

where $P_{\lambda}^{(i)}(s|a) = \text{Tr}[\rho_{\lambda}^{(i)} \hat{\Pi}_{a,s}^{(i)}]$. In a device-independent framework, we do not know the explicit expressions of the projectors $\hat{\Pi}_{a,s}^{(i)}$ corresponding to the measurements which are actually being performed; and even the Hilbert space of the system, over which the quantum state ρ and these projectors are defined, is unknown and arbitrary – it could even be infinite dimensional. Yet, regardless of the actual Hilbert space describing the system, if the state is not entangled, then a decomposition as in Eq. (3) must exist for the experimentally-observed correlations contained in $P(\mathbf{s}|\mathbf{a})$.

Therefore, if conversely $P(\mathbf{s}|\mathbf{a})$ is found to violate a Bell's inequality – denying the possibility to decompose $P(\mathbf{s}|\mathbf{a})$ as in Eq. (3) –, then ρ must be entangled. Crucially, this holds regardless of the Hilbert space of the individual subsystems, and regardless of the measurements which were actually performed to generate $P(\mathbf{s}|\mathbf{a})$. Violating a Bell's inequality therefore certifies that ρ is entangled in a device-independent manner.

Note that in principle, violating a Bell's inequality allows for quantum information protocols more powerful than merely witnessing entanglement [4], which is the task on which we focus in this paper.

B. Permutationally-invariant Bell's inequalities from two-body correlations

Certifying entanglement from two-body correlations. Overall, reconstructing $P(\mathbf{s}|\mathbf{a})$ requires collecting $k^N(d^N - 1)$ probabilities. This exponential scaling clearly makes full reconstruction of these marginals unpractical, and therefore, methods based on partial information have been developed. The simplest non-trivial strategy, which we follow in this paper, is to consider jointly all two-body marginals: $P^{(ij)}(s,t|a,b)$ ($i \neq j$), namely the probability to obtain the pair of outcomes (s,t) if measurement a is performed on subsystem i , and measurement b on subsystem j , for all possible pairs of subsystems $1 \leq i < j \leq N$, and all possible pairs of measurement settings $0 \leq a,b \leq k-1$.

Local-variable models as distributions over classical spin configurations. The *à-la-Bell* formulation of LV models as in Eq. (3) makes transparent the link with entangled quantum states. It is however more intuitive to represent LV models as probability distributions over the measurement results treated as classical variables $s_a^{(i)}$ [9]. Indeed, according to a theorem by A. Fine [4, 15], a LV decomposition as in Eq. (3) exists if and only if there exists a grand-probability distribution $P_{\text{LV}}[\sigma]$ over the fictitious ensemble of classical variables $\sigma = \{s_a^{(i)}\}$, such that the observed statistical properties are obtained as marginals against P_{LV} , i.e. [9, 15]:

$$P_{\text{LV}}^{(ij)}(s,t|a,b) = \sum_{\sigma} P_{\text{LV}}[\sigma] \delta_{s_a^{(i)},s} \delta_{s_b^{(j)},t}, \quad (4)$$

where δ is the Kronecker symbol ($\delta_{x,y} = 1$ if $x = y$, and $= 0$ otherwise). In LV models, measurement results may therefore be viewed as sampled from an underlying classical “spin” configuration σ , where k “hidden” d -level spins $s_a^{(i)} \in \{-j, -j+1, \dots, j\}$ are attached to each subsystem i , encoding the outcome of the measurement. While, at each measurement run with setting $\mathbf{a} = \{a^{(i)}\}_{i=1}^N$, the value of only one of the k hidden spins is revealed [namely, $s_{a^{(i)}}^{(i)}$], in LV models all the unobserved outcomes $[s_b^{(i)}, \text{ for } b \neq a^{(i)}]$ also objectively exist independently of the act of their measurement. This contradicts standard interpretations of quantum physics if they correspond to incompatible quantum observables performed on the same subsystem, $[\hat{s}_a^{(i)}, \hat{s}_b^{(i)}] \neq 0$ – and is categorically excluded if the $P^{(ij)}(s,t|a,b)$ violate a Bell's inequality, and if actions-at-a-distance are not allowed [4].

Permutationally-invariant Bell's inequalities. Deciding whether or not the marginals $P^{(ij)}(s,t|a,b)$ are compatible with a grand-probability $P_{\text{LV}}(\sigma)$ can be mapped onto a so-called inverse Ising problem [9], which can generically be solved in polynomial time by Monte-Carlo methods – while worst-case instances are exponentially hard. A convergent hierarchy of relaxations to this

problem has also been developed, whose computational cost is strictly polynomial at each relaxation level [8]. Here, we drastically simplify the problem by further symmetrizing the data over all permutations of the subsystems [6, 11], which leads us to introduce:

$$\bar{P}(s, t|a, b) = \frac{1}{N(N-1)} \sum_{i \neq j} P^{(ij)}(s, t|a, b) . \quad (5)$$

Bell's inequalities are constraints, of the form:

$$f(\bar{P}_{\text{LV}}) \geq B_c \quad (6)$$

where f is some function, and B_c the so-called classical bound, obeyed by all distributions $\bar{P}_{\text{LV}}(s, t|a, b)$ which descend from a grand-probability $P_{\text{LV}}(\sigma)$. If the particular \bar{P} under investigation happens to violate such a Bell's inequality [namely, if $f(\bar{P}) < B_c$], then no grand-probability $P_{\text{LV}}(\sigma)$ can ever explain the data, which in turn implies that the quantum state ρ of the system must be entangled.

Our main result is to construct a very flexible data-driven algorithm, whose complexity is independent of N , allowing one to build a Bell's inequality violated by the data $\bar{P}(s, t|a, b)$ (Section II A). This allows us to recover all previously known permutationally-invariant Bell's inequalities which are robustly violated by appropriate quantum states in the thermodynamic limit [7, 9], to improve these Bell's inequalities by considering more measurement settings (Section II), and to generalize them to scenarios with arbitrarily-many outcomes (Section III). We discuss the potentialities of several experimental platforms to observe Bell non-locality in Section IV, and draw our conclusions in Section V.

II. TWO-OUTCOMES MEASUREMENTS

Summary of the main results. In this section, we introduce our method by focusing on the simplest situation where the measurements can only deliver $d = 2$ outcomes. The method itself is presented in Section II A: the key results are contained in Eqs. (9), (10) and (11), which form the core of our data-driven algorithm. To be practically useful, the algorithm must be fed with carefully-chosen quantum data. In Section II B, we consider a situation where the data correspond to spin measurements on a collection of quantum spin-1/2. We expose the dependence of these data on collective-spin fluctuations, as represented by Eqs. (14) and (15). We then begin our data-driven exploration of Bell's inequalities with spin singlets (Section II C) and spin-squeezed states (Section II D), for which permutationally-invariant Bell's inequalities are already known. In both cases, we find tighter Bell's inequalities, leading to sufficient “witness” conditions on collective spin fluctuations which are easier to satisfy than existing ones. Concerning singlets (Section II C), our main finding is a family of Bell's inequalities for arbitrarily-many measurement settings [Eq. (16)]. The

corresponding witness condition is contained in Eq. (20). Concerning spin-squeezed states (Section II D), we illustrate the generic improvement offered by the non-linear nature of our Bell's inequalities on Fig. 2. We then go beyond existing Bell's inequalities [6, 7, 12] by adding an extra measurement setting, whose advantage for entanglement certification is illustrated on Figs. 3 and 4.

A. A convex-optimization algorithm

We assume that all measurements $\hat{s}_a^{(i)}$ can only deliver $d = 2$ possible outcomes, denoted $s = \pm 1/2$ (the usual convention in the literature would be to denote them $s = \pm 1$, but we follow our general convention $s \in \{-j, -j+1, \dots, j\}$ with $d = 2j+1$; as already emphasized, these labels are arbitrary). Instead of working with the pair probability distribution $P^{(ij)}(s, t|a, b)$, we equivalently consider one- and two-body correlations $\langle s_a^{(i)} \rangle$ and $\langle s_a^{(i)} s_b^{(j)} \rangle$ (the two representations are related by elementary linear transformations). As coarse-grain features of the experimental data, equivalently to the averaged pair distribution $\bar{P}(s, t|a, b)$, we consider the one- and two-body correlations summed over all permutations of the subsystems:

$$M_a = \sum_{i=1}^N \langle s_a^{(i)} \rangle \quad (7a)$$

$$C_{ab} = \sum_{i \neq j} \langle s_a^{(i)} s_b^{(j)} \rangle . \quad (7b)$$

In a LV description, the $s_a^{(i)}$ are Nk classical Ising spins (with values $\pm 1/2$). A LV model compatible with the (coarse-grain) experimental data corresponds to a probability distribution $P_{\text{LV}}(\{s_a^{(i)}\})$ over the configurations of these Ising spins, such that M_a and C_{ab} are obtained as marginals against P_{LV} . Let us assume that a LV model fitting the data exists, and derive necessary conditions obeyed by the corresponding M_a and C_{ab} (namely, Bell's inequalities). We first introduce the collective variables $S_a = \sum_{i=1}^N s_a^{(i)}$, and their fluctuations $\delta S_a = S_a - \langle S_a \rangle$, so that we have:

$$M_a = \langle S_a \rangle \quad (8a)$$

$$\tilde{C}_{ab} := C_{ab} - M_a M_b = \langle \delta S_a \delta S_b \rangle - \sum_{i=1}^N \langle s_a^{(i)} s_b^{(i)} \rangle . \quad (8b)$$

The terms on the r.h.s of Eq. (8b) are not directly observable. In particular, the terms $\langle s_a^{(i)} s_b^{(i)} \rangle$ correspond to correlations among the measurement settings a and b on the same subsystem i . In the general case, these settings correspond to incompatible quantum observables, $[\hat{s}_a^{(i)}, \hat{s}_b^{(i)}] \neq 0$, and therefore these terms do not have a direct meaning in quantum physics. However, they are perfectly well-defined in LV models. The first key observation, which underlies the method developed in the present

paper, is that for any $k \times k$ positive semi-definite (PSD) matrix $A \succeq 0$, and for any configuration of the collective variables S_a , we have $\sum_{a,b} \delta S_a A_{ab} \delta S_b = \delta \mathbf{S}^T A \delta \mathbf{S} \geq 0$. We introduced the vector notation $\mathbf{S} := (S_0, \dots, S_{k-1})^T$, and used the fact that, by definition of a PSD matrix, $\mathbf{u}^T A \mathbf{u} \geq 0$ for any vector \mathbf{u} . Therefore, for any $A \succeq 0$ and any vector $\mathbf{h} = (h_0, \dots, h_{k-1})^T$, we have:

$$\begin{aligned} \text{Tr}(A\tilde{C}) + \mathbf{h} \cdot \mathbf{M} &= \sum_{a,b} A_{ab} \tilde{C}_{ab} + \sum_a h_a M_a \\ &\geq -\sum_{i=1}^N \left[\sum_{a,b} A_{ab} \langle s_a^{(i)} s_b^{(i)} \rangle - \sum_a h_a \langle s_a^{(i)} \rangle \right] \\ &\geq -N E_{\max}(A, \mathbf{h}), \end{aligned} \quad (9)$$

where $E_{\max}(A, \mathbf{h}) = \max_{\mathbf{s} \in \{\pm 1/2\}^k} [\mathbf{s}^T A \mathbf{s} - \mathbf{h} \cdot \mathbf{s}]$. This is a Bell's inequality, obeyed by all data (C_{ab}, M_a) compatible with LV models, any PSD matrix A , and any vector \mathbf{h} . The bound $E_{\max}(A, \mathbf{h})$ may easily be evaluated by enumerating all 2^k configurations of the \mathbf{s} variables, whenever k (the number of settings) is not too large. The goal is then to find a PSD matrix A and a vector \mathbf{h} such that Eq. (9) is violated. In order to build them, our second key observation is that $E_{\max}(A, \mathbf{h})$ is a convex function of its arguments. A simple proof of convexity, inspired by statistical physics, is to write $E_{\max}(A, \mathbf{h}) = \lim_{\beta \rightarrow \infty} \log Z_\beta(A, \mathbf{h})$, where $Z_\beta(A, \mathbf{h}) = \sum_{\mathbf{s} \in \{\pm 1/2\}^k} \exp[\beta(\mathbf{s}^T A \mathbf{s} - \mathbf{h} \cdot \mathbf{s})]$, and to recognize that $\log Z_\beta$ is a convex function for any β . Furthermore, $\text{Tr}(A\tilde{C}) + \mathbf{h} \cdot \mathbf{M}$, which is a linear function of A and \mathbf{h} , is also convex. Therefore, we may introduce the convex cost function:

$$L(A, \mathbf{h}) = \text{Tr}(A\tilde{C}) + \mathbf{h} \cdot \mathbf{M} + N E_{\max}(A, \mathbf{h}), \quad (10)$$

which by Eq. (9) is non-negative if (C, \mathbf{M}) are compatible with a LV model. Our data-driven algorithm [16] consists therefore in solving the following optimization problem:

$$\begin{aligned} &\text{minimize } L(A, \mathbf{h}) \\ &\text{s.t. } A \succeq 0, \|A\| \leq 1, |\mathbf{h}| \leq 1. \end{aligned} \quad (11)$$

The bounds $\|A\| \leq 1$ and $|\mathbf{h}| \leq 1$ on the norm of A and \mathbf{h} ensure that the optimum is not unbounded below (any other cutoff would work as well). As the PSD constraint $A \succeq 0$ maintains the convex nature of the optimization problem [17], if there exists a Bell's inequality of the form of Eq. (9) which is violated by the data, then we have the guarantee to find the corresponding $A \succeq 0$ and \mathbf{h} s.t. $L(A, \mathbf{h}) < 0$.

Clearly, the possibility to discover new and useful Bell's inequalities via our method crucially depends on the input quantum data $\{C_{ab}, M_a\}$, which must be able to display Bell's non-locality. We will consider a situation where the quantum data are obtained by spin measurements (Sec. II B). In this case, C_{ab} and M_a are completely determined by the first- and second-moments of the collective spin. As a first application, we will recover and improve over the existing Bell's inequalities in scenarios with $d = 2$ outcomes, which are violated by appropriate measurements spin singlets [9] (Sec. II C) and

spin-squeezed states [7] (Sec. II D), and whose violation is robust in the thermodynamic limit. In Section III, we will then generalize these results to scenarios with $d > 2$ outcomes.

B. Spin measurements

Throughout the paper, we investigate the violation of Bell's inequalities when the local measurement settings correspond to spin measurements in the xy -plane, in a direction independent of the subsystem. This allows us to derive simple conditions on the quantum state, involving collective spin fluctuations, which are sufficient to violate the Bell's inequalities if the appropriate measurements are performed (in the literature, such conditions are often referred to as “Bell-correlation witnesses”). We choose therefore:

$$\hat{s}_a^{(i)} = \hat{S}_x^{(i)} \cos \theta_a + \hat{S}_y^{(i)} \sin \theta_a, \quad (12)$$

where $\hat{S}_x^{(i)}$ and $\hat{S}_y^{(i)}$ are local spin observables in directions x and y . $\hat{s}_a^{(i)}$ defines a projective spin measurement along the direction $(\cos \theta_a, \sin \theta_a)$, and has therefore eigenvalues $\pm 1/2$. Introducing the collective spin $\hat{J}_x = \sum_{i=1}^N \hat{S}_x^{(i)}$ and $\hat{J}_y = \sum_{i=1}^N \hat{S}_y^{(i)}$, we also define the collective spin observables:

$$\hat{J}_a = \sum_{i=1}^N \hat{s}_a^{(i)} = \hat{J}_x \cos \theta_a + \hat{J}_y \sin \theta_a. \quad (13)$$

With these conventions, the quantum data used as input of our algorithm, and against which the Bell's inequalities are evaluated, are:

$$M_a = \langle \hat{J}_a \rangle = \langle \hat{J}_x \rangle \cos \theta_a + \langle \hat{J}_y \rangle \sin \theta_a \quad (14a)$$

$$\tilde{C}_{ab} = \Re \langle \delta \hat{J}_a \delta \hat{J}_b \rangle - \frac{N}{4} \cos(\theta_a - \theta_b), \quad (14b)$$

where $\delta \hat{J}_a = \hat{J}_a - M_a$, so that $\Re \langle \delta \hat{J}_a \delta \hat{J}_b \rangle = \langle \hat{J}_a \hat{J}_b + \hat{J}_b \hat{J}_a \rangle / 2 - M_a M_b$ is the covariance of the collective spin observables \hat{J}_a and \hat{J}_b .

When considering input quantum data, we shall assume that the mean spin orientation is along x , so that $\langle \hat{J}_y \rangle = 0$. Finally, we shall assume that off-diagonal correlations vanish: $\langle \hat{J}_x \hat{J}_y \rangle = 0$. Elementary algebra then allows us to express the input data as:

$$M_a = \langle \hat{J}_x \rangle \cos \theta_a \quad (15a)$$

$$\begin{aligned} \tilde{C}_{ab} &= \text{Var}(\hat{J}_x) \cos \theta_a \cos \theta_b + \text{Var}(\hat{J}_y) \sin \theta_a \sin \theta_b \\ &\quad - \frac{N}{4} \cos(\theta_a - \theta_b) \end{aligned} \quad (15b)$$

where we define the variance $\text{Var}(\hat{A}) = \langle \hat{A}^2 \rangle - \langle \hat{A} \rangle^2$.

C. A family of Bell's inequalities for singlet-like correlations

As a first application of our data-driven method, we focus on states with a vanishing mean spin ($\langle \hat{J}_x \rangle = 0$), and derive Bell's inequalities for spin singlets [defined by $\text{Var}(\hat{J}_x) = \text{Var}(\hat{J}_y) = \text{Var}(\hat{J}_z) = 0$]. It is already known that a state is entangled when $\text{Var}(\hat{J}_x) + \text{Var}(\hat{J}_y) < N/4$ [10]. It is also known that $[\langle \hat{J}_x^2 \rangle + \langle \hat{J}_y^2 \rangle]/N < 1/(8+6\sqrt{2}) \approx 0.060660\dots$, which is a more demanding condition, leads to violation of a many-body Bell's inequality [9]. The measurement strategy to maximally violate the Bell's inequality of ref. [9] is composed of k coplanar spin measurements at angles $\theta_a = a\pi/k$. Our main result in this Section is to show that the Bell's inequality of ref. [9] is not the tightest one in this measurement scenario for $k \geq 4$, leading us to discover a new family of Bell's inequalities. We find that Bell-nonlocality can be demonstrated whenever $[\text{Var}(\hat{J}_x) + \text{Var}(\hat{J}_y)]/N < 1/2 - 4/\pi^2 \approx 0.094715$, in the limit of $k \rightarrow \infty$.

Bell's inequality. As input quantum data, we consider a perfect spin singlet, for which $M_a = 0$ and $4\tilde{C}_{ab}/N = -\cos[\theta_a - \theta_b] = -\cos[\pi(a - b)/k]$ [from Eq. (15)]. Applying our algorithm to these data for up to $k = 10$, we find that the following Bell's inequality is violated:

$$\langle \mathcal{B} \rangle = \sum_{a,b=0}^{k-1} \tilde{C}_{ab} \cos[\pi(a - b)/k] \quad (16)$$

$$\geq -N \max_{\mathbf{s} \in \{\pm 1/2\}^k} \sum_{a,b=0}^{k-1} s_a s_b \cos[\pi(a - b)/k] \quad (17)$$

$$= -\frac{N}{4 \sin^2[\pi/(2k)]} := B_c, \quad (18)$$

where on the second line we used Eq. (9). The classical bound B_c is obtained by noting that $\sum_{a,b=0}^{k-1} s_a s_b \cos[\pi(a - b)/k] = \left| \sum_{a=0}^{k-1} s_a e^{ia\pi/k} \right|^2$. The maximum is obtained by choosing all $s_a = 1/2$, and is $1/[4 \sin^2[\pi/(2k)]]$.

Quantum violation. To evaluate Eq. (16) against a generic quantum state [Eq. (14)], we first introduce the matrix $A_{ab} = \cos[\pi(a - b)/k]$. Using $A_{ab} = \Re[e^{ia\pi/k} e^{-ib\pi/k}]$, the matrix A is diagonalized as $A = (k/2)(\mathbf{c} \cdot \mathbf{c}^T + \mathbf{s} \cdot \mathbf{s}^T)$ with the normalized vectors $\mathbf{c}^T = \sqrt{2/k}[\cos(a\pi/k)]_{a=0}^{k-1}$ and $\mathbf{s}^T = \sqrt{2/k}[\sin(b\pi/k)]_{a=0}^{k-1}$. To evaluate $\sum_{ab} \hat{J}_a A_{ab} \hat{J}_b$, we first compute $\sum_{a=0}^{k-1} c_a \hat{J}_a = \sqrt{2/k} \sum_{a=0}^{k-1} \cos(a\pi/k) [\cos(a\pi/k) \hat{J}_x + \sin(a\pi/k) \hat{J}_y] = \sqrt{k/2} \hat{J}_x$. Similarly, we find $\sum_{a=0}^{k-1} s_a \hat{J}_a = \sqrt{k/2} \hat{J}_y$. Fi-

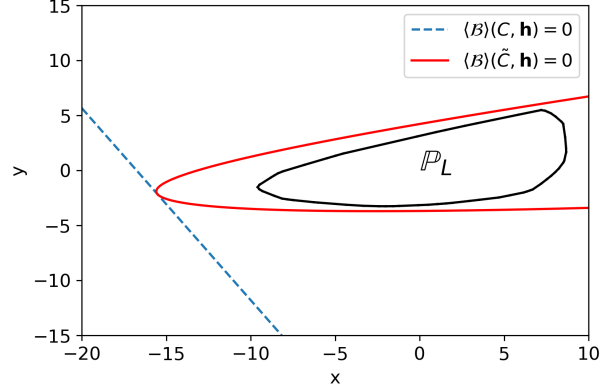


FIG. 2: The (non-linear) Bell's inequalities obtained with our method, which involve \tilde{C}_{ab} [Eq. (8b)], are tighter than standard (linear) Bell's inequalities which involve C_{ab} [Eq. (7b)]. Here, this is illustrated for $N = 10$ for the Bell's inequality of Eq. (21) [6, 7]. We sliced the 5-dimensional space $(M_0, M_1, C_{00}, C_{01} = C_{10}, C_{11})$ along a randomly-chosen $2d$ plane; x and y are the coordinates within this $2d$ plane. The convex black region \mathbb{P}_L is the polytope of LV models, the dashed blue line is the linear Bell's inequality of refs. [6, 7], and the red solid line is the corresponding non-linear Bell's inequality of Eq. (21), constructed from the \tilde{C}_{ab} correlations.

nally, using $\sum_{a,b=0}^{k-1} \cos^2[\pi(a - b)/k] = k^2/2$, we find:

$$\sum_{a,b=1}^k \tilde{C}_{ab} \cos[\pi(a - b)/k] = \frac{k^2}{4} [\text{Var}(\hat{J}_x) + \text{Var}(\hat{J}_y)] - \frac{Nk^2}{8}. \quad (19)$$

Violation of the Bell's inequality is therefore detected whenever:

$$\frac{1}{N} [\text{Var}(\hat{J}_x) + \text{Var}(\hat{J}_y)] < \frac{1}{2} - \frac{1}{k^2 \sin^2(\pi/2k)}. \quad (20)$$

The tightest condition is achieved in the limit $k \rightarrow \infty$, yielding the bound $1/2 - 4/\pi^2$. Notice that the condition of Eq. (20) is tighter than the one derived in ref. [9], not only because the r.h.s is larger – and therefore detecting more data as exhibiting Bell's non-locality in the same measurement scenario –, but also because it involves variances of the collective operators, making the condition easier to satisfy [indeed, $\text{Var}(\hat{A}) = \langle \hat{A}^2 \rangle - \langle \hat{A} \rangle^2 \leq \langle \hat{A}^2 \rangle$] – see the related Fig. 2.

D. Spin-squeezed states

Spin-squeezed states of N two-level systems represent paradigmatic many-body entangled states, and are a central resource for quantum-enhanced interferometry [18].

State-of-the-art Bell's inequality. In the context of Bell's non-locality, spin-squeezing is known to be es-

sentential for the robust violation of the following Bell's inequality involving $k = 2$ measurement settings per subsystem [6, 7, 12, 19]:

$$\langle \mathcal{B} \rangle = \tilde{C}_{00} + \tilde{C}_{11} - \tilde{C}_{01} - \tilde{C}_{10} - (M_0 + M_1) \geq -N . \quad (21)$$

Notice that we are using the convention that the outcomes are $\pm 1/2$, different from the convention ± 1 used in the above-cited papers; this explains why the coefficients of Eq. (21) are different. Notice also that in the literature, the Bell's inequality involves the correlations C_{ab} [Eq. (7b)], and not $\tilde{C}_{ab} = C_{ab} - M_a M_b$ [Eq. (8b)]. Using \tilde{C}_{ab} in Eq. (21) includes the extra term $-(M_0 - M_1)^2 \leq 0$ as compared to the literature, and therefore represents already a tighter Bell's inequality – see Fig. 2 for an illustration. Since this extra term is of order $O(N^2)$ while the classical bound is $O(N)$, the relative improvement generically grows with N .

The classical bound is found, following Eq. (9), by writing $\mathcal{B} = (\delta S_0 - \delta S_1)^2 - \sum_{i=1}^N [(s_0 - s_1)^2 + s_0 + s_1]^{(i)}$, and noting that $(s_0 - s_1)^2 + s_0 + s_1 \geq -1$ for all possible values of $s_0, s_1 = \pm 1/2$. This Bell's inequality can be violated by preparing a spin-squeezed state, defined by $N\text{Var}(\hat{J}_y) < \langle \hat{J}_x \rangle^2$ [18], and performing two projective spin measurements in directions $\hat{s}_a^{(i)} = \hat{S}_x^{(i)} \cos \theta \pm \hat{S}_y^{(i)} \sin \theta$ [7, 19]. Computing the quantum value [e.g. from Eq. (15)], we obtain $\langle \mathcal{B} \rangle = 4\sin^2 \theta \text{Var}(\hat{J}_y) - 2\cos \theta \langle \hat{J}_x \rangle - N\sin^2 \theta$. The optimal angle θ , minimizing $\langle \mathcal{B} \rangle$ for fixed data $(\text{Var}(\hat{J}_y), \langle \hat{J}_x \rangle)$, is $\cos \theta = \langle \hat{J}_x \rangle / [N - 4\text{Var}(\hat{J}_y)]$. For this choice of measurements, we obtain $\langle \mathcal{B} \rangle = -N + 4\text{Var}(\hat{J}_y) - \langle \hat{J}_x \rangle^2 / [N - 4\text{Var}(\hat{J}_y)]$. For perfect squeezed states [$\text{Var}(\hat{J}_y) \rightarrow 0, \langle \hat{J}_x \rangle \rightarrow N/2$], we can obtain violation up to $\langle \mathcal{B} \rangle = -5N/4$. In this Section, we show that the robustness of Bell non-locality detection for spin-squeezed states can be improved by considering extra measurements ($k \geq 3$).

Finding tightest and more robust Bell's inequalities. To find better Bell's inequalities, our strategy was to consider quantum data [Eq. (15)] obtained from a squeezed state at the limit of violating the Bell's inequality Eq. (21), and add extra measurements in the xy -plane to potentially discover other violated Bell's inequalities. In particular, adding a third spin measurement $\hat{S}_y^{(i)}$ along the y -axis, we found a family of Bell's inequalities, defined by the following coefficients [see Eq. (9)]:

$$A = \begin{pmatrix} 1 & -1 & a \\ -1 & 1 & -a \\ a & -a & a^2 \end{pmatrix} \quad (22a)$$

$$\mathbf{h}^T = -(1+a, 1+a, 0) , \quad (22b)$$

where $a \geq 0$. The corresponding Bell's inequality reads:

$$\langle \mathcal{B} \rangle = \text{Tr}(A\tilde{C}) + \mathbf{h} \cdot \mathbf{M} \geq -N(1+a/2)^2 := B_c , \quad (23)$$

and reduces to Eq. (21) when $a = 0$. Noting that $\mathbf{x}^T A \mathbf{x} =$

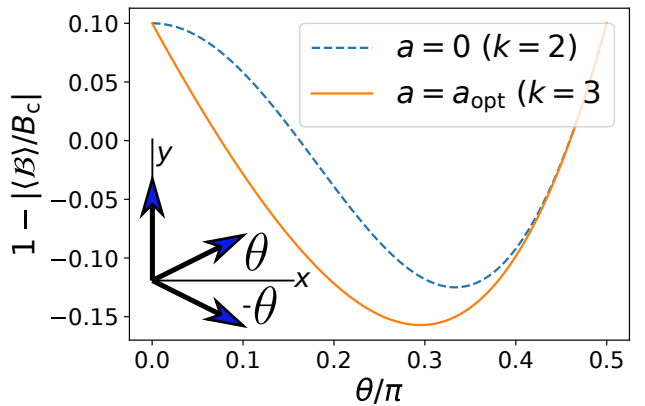


FIG. 3: Bell's inequality violation for $j = 1/2$ spin-squeezed states, as a function of the measurement angle θ . Dashed line: relative violation of the Bell's inequality of Eq. (21), which involves $k = 2$ measurement settings at angles $\pm \theta$. Solid line: relative violation of the Bell's inequality of Eq. (23), which involves a third measurement along the y -axis (see the sketch on the bottom-left corner), for the optimal value of the parameter a defining the Bell's inequality. The quantum state has a mean spin $2\langle \hat{J}_x \rangle / N = m_x = 0.9$, and transverse collective-spin fluctuations $4\text{Var}(\hat{J}_y) / N = \chi^2 = 0.1$. For both inequalities, the absolute value of the relative violation is equal to the amount of white noise tolerated by the data to observe a non-zero violation (see text).

$(x_0 - x_1 + ax_2)^2$ for any vector \mathbf{x} , we may write:

$$\mathcal{B} = [\delta(S_0 - S_1 + aS_2)]^2 - \sum_{i=1}^N \{ (1+a)[s_0 + s_1] + [s_0 - s_1 + as_2]^2 \}^{(i)} . \quad (24)$$

The classical bound $B_c = -N(1+a/2)^2$ is then found by enumerating the configurations of the variables $s_a^{(i)} = \pm 1/2$. On the other hand, in the quantum measurement setting we consider, we find:

$$\langle \mathcal{B} \rangle = [\text{Var}(\hat{J}_y) - N/4](a + 2\sin \theta)^2 - 2(1+a)\langle \hat{J}_x \rangle \cos \theta . \quad (25)$$

The quantum data (\tilde{C}_{ab}, M_a) being fixed, it is then natural to consider the optimal values of θ and a to have the most robust violation of the Bell's inequality. If white noise is added to the data, then $(C_{ab}, M_a) \rightarrow (1-r)(C_{ab}, M_a)$ with r the noise amplitude. If we assume that $\langle \hat{J}_y \rangle = 0$, so that $\text{Var}(\hat{J}_y) = \langle \hat{J}_y^2 \rangle$, then correspondingly $\langle \mathcal{B} \rangle \rightarrow (1-r)\langle \mathcal{B} \rangle$. Maximizing the noise robustness is therefore equivalent to maximizing the ratio $|\langle \mathcal{B} \rangle / B_c| = [(1+a)m_x \cos \theta + (1-\chi^2)(a/2 + \sin \theta)^2] / (1+a/2)^2$, where we introduced $m_x = 2\langle \hat{J}_x \rangle / N$ (the Rabi contrast [7]) and $\chi^2 = 4\text{Var}(\hat{J}_y) / N$ the scaled second moment. For each value of θ , we may then find the value of a which maximizes this ratio. As illustrated on Fig. 3 for $m_x = 0.9$ and $\chi^2 = 0.1$, adding a third measurement along the y -axis and optimizing over the parameter a yields a systematic improvement over Eq. (21).

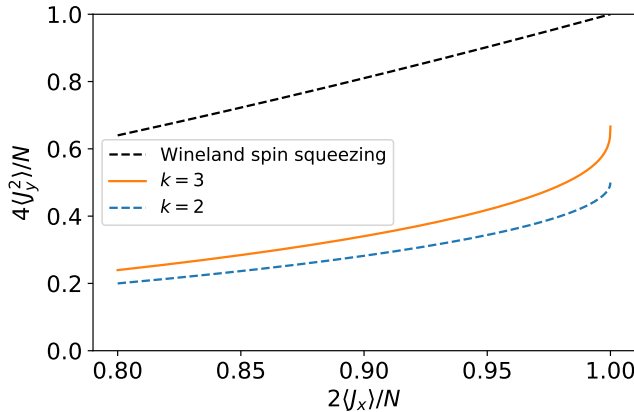


FIG. 4: Entanglement detection for $j = 1/2$ spin-squeezed states. Below each line, the corresponding entanglement criterion is violated. Dashed black line: Wineland spin squeezing criterion; solid orange line: violation of the new Bell's inequality Eq. (23); dashed blue line: violation of the Bell's inequality Eq. (21).

Finally, for given values of (m_x, χ^2) , we may find the measurement angle θ which maximizes the robustness of the violation of Eq. (23). This is done on Fig. 4, which shows the parameter regime in the (m_x, χ^2) where Bell non-locality is detected. For comparison we also plot the regime where non-locality is detected based on the violation of Eq. (21), and where entanglement is detected based on the Wineland spin squeezing criterion $m_x^2 > \chi^2$. The Bell's inequality with $k = 3$ settings extends by about 20% the parameter space where non-locality can be detected.

Further improvement. Even more robust Bell's inequalities may be found by considering $k \geq 2$ pairs of measurements in the xy plane, in directions $\hat{s}_a^{(i)} = \hat{S}_x^{(i)} \cos \theta_a + \hat{S}_y^{(i)} \sin \theta_a$ and $[\hat{s}_a^{(i)}]' = \hat{S}_x^{(i)} \cos \theta_a - \hat{S}_y^{(i)} \sin \theta_a$, and one measurement along y denoted $\hat{s}_k^{(i)} = \hat{S}_y^{(i)}$. In this Bell scenario with $2k+1$ settings applied to spin-squeezed states, this generically leads to Bell' inequalities of the form:

$$\begin{aligned} & \left[\sum_{a=0}^{k-1} \alpha_a (S_a - S'_a) + S_k \right]^2 - \sum_{i=1}^N \{ \\ & \sum_{a=0}^{k-1} \beta_a (s_a + s'_a) + \left[\sum_{a=0}^{k-1} \alpha_a (s_a - s'_a) + s_k \right]^2 \}^{(i)} \\ & \geq B_c \quad (26) \end{aligned}$$

for some data-tailored coefficients α_a and β_a . Similarly as in the previous paragraph, for given values of (m_x, χ^2) , it is then possible to numerically optimize over the measurement angles θ_a in order to maximize the violation robustness.

III. ARBITRARY-OUTCOMES MEASUREMENTS

Summary of the main results. In the previous section, we focused on measurements with $d = 2$ outcomes – and considered a physical implementation with spin-1/2 measurements. In this section, we extend these results to arbitrarily-many outcomes ($d > 2$), corresponding to the physical situation where spin measurements are performed on individual spin- j components (with $d = 2j+1$). Sec. III A presents an incremental generalization of the algorithm of Sec. II A, which incorporates an extra feature of the quantum data [Eq. (27)]. This turns out to be an essential ingredient to generalize the Bell's inequalities of the previous section. We first consider spin- j singlets in Sec. III B, and restrict our attention to $k = 3$ spin measurements in a given plane. We unveil an increasingly complex situation for $j > 1/2$, as illustrated on Fig. 5, with $2j$ inequivalent Bell's inequalities, already in this simple setting. We could however characterize analytically two families of Bell's inequalities which emerged from our algorithm (Sec. III B 2). One of them extends Eq. (16) to arbitrary half-integer spins (for $k = 3$ measurements), and the corresponding witness condition is given by Eq. (38). The other family is valid for both integer and half-integer spins, and the witness condition is given by Eq. (40). We conclude our exploration in Sec. II D with spin- j squeezed states. Our main result is a generalization of the Bell's inequality of Eq. (21) to arbitrary $j \geq 1/2$ [Eq. (41)]. The corresponding witness condition for spin- j squeezed states is given by Eq. (43).

A. Algorithm tailored to spin measurements

We consider the general scenario in which the local measurements $\hat{s}_a^{(i)}$ ($a \in \{0, \dots, k-1\}$, $i \in \{1, \dots, N\}$) can deliver $d \geq 2$ possible outcomes, denoted $s = \{-j, -j+1, \dots, j\}$ with $d = 2j+1$. In general, the pair probability distribution $P^{(ij)}(s, t|a, b)$ may be reconstructed from the single-body expectation values $\langle [s_a^{(i)}]^\alpha \rangle$ with $\alpha \in \{1, \dots, d-1\}$, and two-body correlations $\langle [s_a^{(i)}]^\alpha [s_b^{(j)}]^\beta \rangle$ with $\alpha, \beta \in \{1, \dots, d-1\}$. The averaged pair probability distribution $\bar{P}(s, t|a, b) = [N(N-1)]^{-1} \sum_{i \neq j} P^{(ij)}(s, t|a, b)$ may then be obtained by averaging over all permutations of the subsystems. In Appendix A, we give a general formulation of our data-driven algorithm for finding a Bell's inequality violated by \bar{P} . However, aiming at finding new Bell's inequalities for many-spin systems with $j > 1/2$, we found sufficient to include only:

$$M_a^{(2)} = \sum_{i=1}^N \langle [s_a^{(i)}]^2 \rangle \quad (27)$$

as an extra coarse-grain feature of the quantum data, in addition to M_a and C_{ab} defined in Eq. (7). Apart

from this modification, we may then follow the same construction as in Section II A, where the kN local classical variables $s_a^{(i)}$ can now take the d possible values $-j, -j+1, \dots, j$. The analogue of Eq. (9) now contains an extra term $\mathbf{h}^{(2)} \cdot \mathbf{M}^{(2)}$ to allow for Bell's inequalities involving this extra feature of the data. Explicitly, for any PSD matrix A , and any vectors $\mathbf{h} = (h_1, \dots, h_k)$ and $\mathbf{h}^{(2)} = (h_1^{(2)}, \dots, h_k^{(2)})$, we have:

$$\begin{aligned} & \text{Tr}(A\tilde{C}) + \mathbf{h} \cdot \mathbf{M} + \mathbf{h}^{(2)} \cdot \mathbf{M}^{(2)} \\ &= \sum_{a,b} A_{ab} \tilde{C}_{ab} + \sum_a h_a M_a + \sum_a h_a^{(2)} M_a^{(2)} \\ &\geq -\sum_{i=1}^N \left\langle \sum_{a,b} A_{ab} s_a^{(i)} s_b^{(i)} - \sum_a h_a s_a^{(i)} - \sum_a h_a^{(2)} [s_a^{(i)}]^2 \right\rangle \\ &\geq -N E_{\max}(A, \mathbf{h}, \mathbf{h}^{(2)}) , \end{aligned} \quad (28)$$

where now $E_{\max}(A, \mathbf{h}, \mathbf{h}^{(2)}) = \max_{\mathbf{s} \in \{-j, \dots, j\}^k} E(\mathbf{s})$, with $E(\mathbf{s}) = \sum_{ab} A_{ab} s_a s_b - \sum_a [h_a s_a + h_a^{(2)} s_a^2]$. Eq. (28) is a Bell's inequality, satisfied by all data M_a , $M_a^{(2)}$ and C_{ab} compatible with a LV model with d -outcome measurements. We may then parallel the end of Section II A: introduce the convex cost function $L(A, \mathbf{h}, \mathbf{h}^{(2)}) = \text{Tr}(A\tilde{C}) + \mathbf{h} \cdot \mathbf{M} + \mathbf{h}^{(2)} \cdot \mathbf{M}^{(2)} + N E_{\max}(A, \mathbf{h}, \mathbf{h}^{(2)})$, and minimize it via a convex-optimization routine, imposing the PSD constraint $A \succeq 0$. If we find $L < 0$, a violated Bell's inequalities is then reconstructed from the corresponding A , \mathbf{h} and $\mathbf{h}^{(2)}$.

Applying this algorithm, we discovered Bell's inequalities violated by spin- j spin singlets, and by spin- j squeezed states. These Bell's inequalities generalize the results of Section II to arbitrary $j \geq 1/2$.

B. Spin singlets

We start our investigation of many-body spin- j systems with states obeying $SU(2)$ rotational invariance: $\langle \hat{J}_x \rangle = \langle \hat{J}_y \rangle = \langle \hat{J}_z \rangle = 0$, and $\langle \hat{J}_x^2 \rangle = \langle \hat{J}_y^2 \rangle = \langle \hat{J}_z^2 \rangle$. Furthermore, as a consequence of $[\hat{S}_x^{(i)}]^2 + [\hat{S}_y^{(i)}]^2 + [\hat{S}_z^{(i)}]^2 = j(j+1)$, we have $[\hat{S}_x^{(i)}]^2 = j(j+1)/3$ for all $i = 1, \dots, N$. We have considered $k = 3$ coplanar spin measurements, in directions $\hat{s}_0^{(i)} = \hat{S}_x^{(i)} \cos \theta + \hat{S}_y^{(i)} \sin \theta$, $\hat{s}_1^{(i)} = \hat{S}_x^{(i)}$, and $\hat{s}_2^{(i)} = \hat{S}_x^{(i)} \cos \theta' + \hat{S}_y^{(i)} \sin \theta'$. We did not find violated Bell's inequalities with $k = 2$ settings, and using non-coplanar spin measurements did not lead to more robust Bell's inequalities. However, we do not exclude that better Bell's inequalities could be found using non-coplanar measurements, with $k \geq 4$ settings, or including more general $SU(2j+1)$ measurements. In summary, this setting appeared as the simplest one to discover new Bell's inequalities, and even in this simplest scenario we could not characterize all the Bell's inequalities which appear when increasing j . Fig. 5 summarizes our findings, where we plot the violation of Bell's inequalities in the $(\theta, -\theta')$ plane, for $j \in \{1/2, 1, 3/2, 2\}$,

together with the witness condition on the collective spin variance $\text{Var}(\hat{J}_x)$ to observe violation (assuming global $SU(2)$ invariance). We shall discuss in details two families of Bell's inequalities, which were characterized analytically for arbitrary j . We begin with general considerations on the Bell's inequalities we found for $SU(2)$ -invariant spin systems.

1. General considerations

Quantum data. As a consequence of $SU(2)$ invariance, the quantum data \tilde{C}_{ab} , M_a and $M_a^{(2)}$ [defined through Eqs. (8) and (27)] are:

$$\tilde{C}_{ab} = [\text{Var}(\hat{J}_x) - Nj(j+1)/3] \cos(\theta_a - \theta_b) \quad (29a)$$

$$M_a = 0 \quad (29b)$$

$$M_a^{(2)} = Nj(j+1)/3 , \quad (29c)$$

where in the present case, $\theta_0 = \theta$, $\theta_1 = 0$ and $\theta_2 = \theta'$.

Structure of the Bell's inequalities. As a consequence of $M_a = 0$, the Bell's inequalities do not involve terms linear in M_a [namely, in the notations of Eq. (28), we have $\mathbf{h} = 0$], and they take the general form:

$$\langle \mathcal{B} \rangle = \sum_{ab} A_{ab} \tilde{C}_{ab} + \sum_a h_a^{(2)} M_a^{(2)} \geq B_c , \quad (30)$$

where A is a symmetric PSD matrix. For LV models, we have:

$$\begin{aligned} \mathcal{B}_{\text{LV}} &= \sum_{ab} \delta S_a A_{ab} \delta S_b - \sum_i \sum_{ab} s_a^{(i)} [A_{ab} - h_a^{(2)} \delta_{ab}] s_b^{(i)} \\ &\geq -N E_{\max}(\tilde{A}) , \end{aligned} \quad (31)$$

where we defined $\tilde{A}_{ab} = A_{ab} - h_a^{(2)} \delta_{ab}$, and:

$$E_{\max}(\tilde{A}) := \max_{\{s_a\} \in \{-j, \dots, j\}^k} \sum_{ab} s_a \tilde{A}_{ab} s_b . \quad (32)$$

Notice that the bound is tight for N even. Indeed, if $\{s_a^{(\text{opt})}\}_{a=0}^{k-1}$ is a configuration saturating E_{\max} , then $\{-s_a^{(\text{opt})}\}_{a=0}^{k-1}$ is also saturating E_{\max} . We may therefore always choose $S_a = \sum_{i=1}^N s_a^{(i)} = 0$, while saturating the bound, by choosing the configuration $\{s_a^{(\text{opt})}\}_{a=0}^{k-1}$ for $N/2$ subsystems, and $\{-s_a^{(\text{opt})}\}_{a=0}^{k-1}$ for the other $N/2$ subsystems.

Quantum value. Considering the quantum value, we find instead:

$$\begin{aligned} \langle \mathcal{B} \rangle &= \text{Var}(\hat{J}_x) \sum_a h_a^{(2)} + \\ &[\text{Var}(\hat{J}_x) - \frac{Nj(j+1)}{3}] \sum_{ab} \tilde{A}_{ab} \cos(\theta_a - \theta_b) \end{aligned} \quad (33)$$

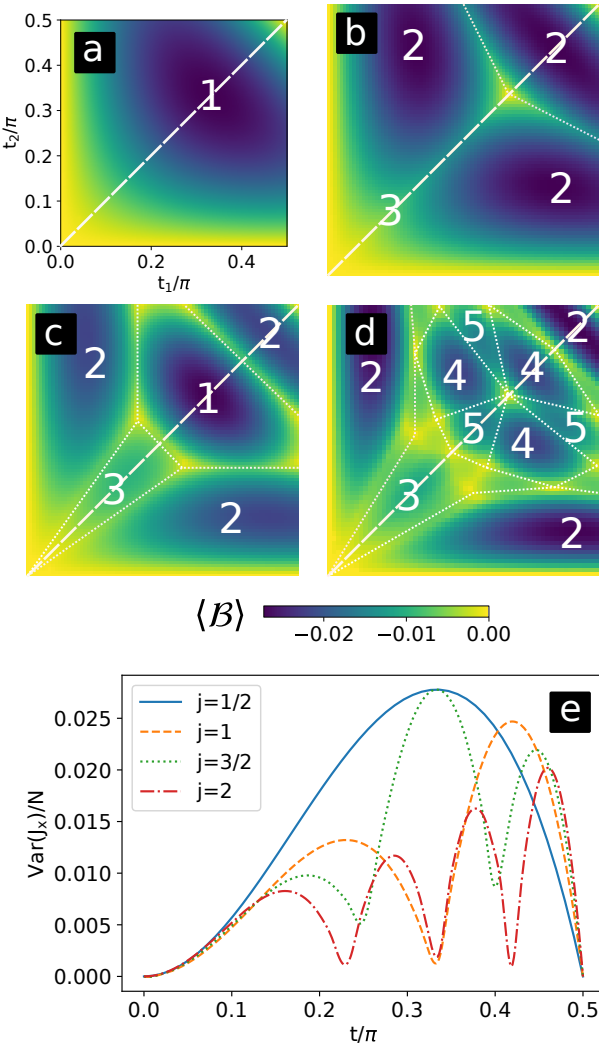


FIG. 5: Bell's inequalities for many-body spin singlets. As input quantum data [Eqs. (29)] to our algorithm, we considered $k = 3$ spin measurements in the xy -plane, forming angles $-t_2$, 0, and t_1 with the x axis. We found violated Bell's inequalities as in Eq. (30), with a conventional normalization $\sum_{ab} A_{ab}^2 + \sum_a [h_a^{(2)}]^2 = 1$, and a classical bound given by Eq. (32). (a,b,c,d): Difference between the classical bound and the quantum value [Eq. (34)], divided by N . (a) $j = 1/2$; (b) $j = 1$; (c) $j = 3/2$; (d) $j = 2$. The integers 1–5 label inequivalent families of Bell's inequalities, which are found in the different regions of parameters (t_1, t_2) (boundaries between these regions are indicated as dotted white lines). In general, we find $2j$ Bell's inequalities inequivalent under relabelling of the outcomes. Labels 1 and 2 respectively correspond to the coefficients of Eqs. (37) and (39). (e) Along $t := t_1 = t_2$ [white dashed line on panels (a-d)], bound on $\text{Var}(\hat{J}_x)/N$ to observe Bell non-locality in this measurement setting [$\langle \mathcal{B} \rangle < -NE_{\text{max}}$ with $\langle \mathcal{B} \rangle$ given by Eq. (33) and E_{max} by Eq. (32)]. The maximum at $t = \pi/3$ for half-integer spins corresponds to label 1, and the witness condition is that of Eq. (38). The right-most local maximum at $t = \arccos[1/(4j)]$ corresponds to label 2, and the witness condition is that of Eq. (40).

Using that $\tilde{A}_{ab} = \tilde{A}_{ba}$, we have $\sum_{ab} \tilde{A}_{ab} \cos(\theta_a - \theta_b) = \sum_{ab} e^{-i\theta_a} \tilde{A}_{ab} e^{i\theta_b}$. Furthermore, for perfect spin singlets, we have $\text{Var}(\hat{J}_x) = 0$, so that:

$$\langle \mathcal{B} \rangle_{\text{singlet}} = -\frac{Nj(j+1)}{3} \sum_{ab} e^{-i\theta_b} \tilde{A}_{ab} e^{i\theta_a}. \quad (34)$$

The optimal angles, leading to the maximal violation of the Bell's inequalities, are those which maximize $\sum_{ab} e^{-i\theta_b} \tilde{A}_{ab} e^{i\theta_a}$. We therefore define:

$$Q_{\text{max}}(\tilde{A}) := \max_{\{\theta_a\} \in [-\pi, \pi]^k} \sum_{ab} e^{-i\theta_b} \tilde{A}_{ab} e^{i\theta_a}. \quad (35)$$

This should be contrasted to the case of LV models where, in order to find the classical bound, one maximizes $\sum_{ab} s_a \tilde{A}_{ab} s_b$ over the variables $s_a \in \{-j, \dots, j\}$ [see Eq. (32)].

On Fig. 5(a-d), we plot the quantum violation of Bell's inequalities by many-body spin singlets, for $j \in \{1/2, 1, 3/2, 2\}$, with $k = 3$ spin-measurement directions. In general, varying the measurement angles in a given plane, we find $2j$ inequivalent inequalities. We characterized analytically one Bell's inequality appearing for all half-integers j , and one family appearing for all j (see below).

Witness condition. From Eq. (33), we can establish the following witness condition on the variance of the collective spin:

$$\frac{\text{Var}(\hat{J}_x)}{N} < \frac{[j(j+1)/3]Q_{\text{max}}(\tilde{A}) - E_{\text{max}}(\tilde{A})}{\sum_a h_a^{(2)} + Q_{\text{max}}(\tilde{A})}. \quad (36)$$

Whenever this condition is satisfied, this establishes (under the assumption of global $SU(2)$ invariance), that the quantum state violates the considered Bell's inequality if the Bell experiment with optimal measurement angles is realized. Such conditions, where $Q_{\text{max}}(\tilde{A})$ is replaced by $\sum_{ab} e^{-i\theta_b} \tilde{A}_{ab} e^{i\theta_a}$ with $\{\theta_a\} = \{-t, 0, t\}$ (not necessarily optimal), are plotted on Fig. 5(e) for $j \in \{1/2, 1, 3/2, 2\}$.

2. Bell's inequalities for arbitrary- j many-body singlets

A Bell's inequality for half-integer spin singlets. The Bell's inequality presented in Eq. (16), and valid for $j = 1/2$, can be extended to arbitrary spins. Here, we focus on the simplest extension with $k = 3$ measurement settings, which corresponds to the region labelled '1' on panels (a) and (c) of Fig. 5. The coefficients are:

$$\tilde{A} = \begin{pmatrix} -1 & 1 & -1 \\ 1 & -1 & 1 \\ -1 & 1 & -1 \end{pmatrix} \quad (37a)$$

$$h^{(2)} = (3, 3, 3). \quad (37b)$$

We notice that for arbitrary complex numbers x_0, x_1, x_2 , we have: $\sum_{ab} x_a^* \tilde{A}_{ab} x_b = -|x_0 - x_1 + x_2|^2 \leq 0$. For integer spins, choosing $s_0 = s_1 = s_2 = 0$ gives $E_{\max} = 0$, so that the classical bound cannot be violated by measuring spin singlets [Eq. (34)]. In contrast, for half-integer spins, the minimal value of $|s_0 - s_1 + s_2|$ is $1/2$, so that $E_{\max} = -1/4$. Instead, choosing the measurement angles $(\pi/3, 0, -\pi/3)$ (which is optimal), we find $\sum_{ab} e^{-i\theta_a} \tilde{A}_{ab} e^{i\theta_b} = 0$. From Eq. (33), the quantum value is therefore $\langle \mathcal{B} \rangle = \text{Var}(\hat{J}_x) \sum_a h_a^{(2)} = 9\text{Var}(\hat{J}_x)$. Violation of the Bell's inequality Eq. (30), with coefficients given by Eq. (37), and whose classical bound is $B_c = N/4$, is therefore possible whenever:

$$\text{Var}(\hat{J}_x) < \frac{N}{36}. \quad (38)$$

We recall that, in order to reach this conclusion, we assumed that the state obeys $SU(2)$ rotational invariance, and that j is a half-integer. This generalizes a result of ref. [9] to arbitrary half-integer spins. On Fig. 5(e), this condition corresponds to the maximum at $t = \pi/3$ for $j \in \{1/2, 3/2\}$.

A family of Bell's inequalities for arbitrary spin singlets. The second family of Bell's inequalities we have characterized is violated for arbitrary j , and corresponds to the region labelled '2' on panels (b,c,d) of Fig. 5. The coefficients of the Bell's inequality are:

$$\tilde{A} = 2j \begin{pmatrix} -2j & 1 & -2j \\ 1 & 0 & 1 \\ -2j & 1 & -2j \end{pmatrix} \quad (39a)$$

$$h^{(2)} = 8j^2(1, 1, 1) + (1, 0, 1). \quad (39b)$$

In this case, for arbitrary complex numbers x_0, x_1, x_2 , we have: $(2j)^{-1} \sum_{ab} x_a^* \tilde{A}_{ab} x_b = x_1^*(x_0 + x_2) + (x_0^* + x_2^*)[x_1 - 2j(x_0 + x_2)]$. The classical bound is $B_c = 0$. Indeed, replacing the complex variables x_a by the variables $s_a \in \{-j, \dots, j\}$, we find $E/(2j)^2 := (s_0 + s_2)[s_1/j - (s_0 + s_2)] \leq 0$. This quantity is only ≥ 0 when $s_0 + s_2$ is between 0 and s_1/j . But since $|s_1/j| \leq 1$, and since $s_0 + s_2$ is always an integer, we conclude that $E_{\max}(\tilde{A}) = 0$. Concerning the quantum value, the optimal choice is $\theta_0 = -\theta_2 = \arccos[1/(4j)]$, and $\theta_1 = 0$, for which we obtain $\sum_{ab} e^{i\theta_a} \tilde{A}_{ab} e^{i\theta_b} = 1$. From Eq. (33), and using the value of $h^{(2)}$ [Eq. (39b)], we finally obtain the quantum value $\langle \mathcal{B} \rangle = -Nj(j+1)/3 + 3(1+8j^2)\text{Var}(\hat{J}_x)$. Violation of the Bell's inequality is achieved when $\langle \mathcal{B} \rangle < 0$, which is the case whenever:

$$\frac{\text{Var}(\hat{J}_x)}{N} < \frac{j(j+1)}{9(1+8j^2)}. \quad (40)$$

In contrast to Eq. (38), this condition is valid for arbitrary j , and only assumes $SU(2)$ invariance of the state. Notice that for $j = 1/2$, this bound is the same as Eq. (38), while it is more demanding for $j > 1/2$ [in the

limit of $j \rightarrow \infty$, it reads $\text{Var}(\hat{J}_x) < N/72$]. On Fig. 5(e), this condition corresponds to the right-most maximum at $t = \arccos[1/(4j)]$.

Further improvement. The Bell's inequalities reported here are the simplest ones discovered via our data-driven method, involving only $k = 3$ co-planar spin measurements. Adding extra measurements, possibly genuine $SU(d)$ measurements, can only lead to more robust Bell's inequalities, and looser witness conditions than Eqs. (38) and (40). We leave this exploration open to future studies, for which our algorithm [16] represents a natural starting point.

C. Spin-squeezed states

A Bell's inequality for arbitrary-spin squeezed states with two settings. Similarly to the measurement scenario leading to the violation of Eq. (21) for spin-1/2 squeezed states, we consider a situation where two projective spin measurements, $s_a^{(i)} = \hat{S}_x^{(i)} \cos \theta \pm \hat{S}_y^{(i)} \sin \theta$, are locally performed on a collection of N spin- j particles. Using data from a spin- j squeezed state, we find the following generalization of Eq. (21):

$$\langle \mathcal{B} \rangle = \tilde{C}_{00} + \tilde{C}_{11} - \tilde{C}_{01} - \tilde{C}_{10} + 2M_0^{(2)} + 2M_1^{(2)} - M_0 - M_1 \geq 0. \quad (41)$$

For $j = 1/2$, we have $M_a^{(2)} = N/4$, and therefore recover Eq. (21). More generally, the classical bound ≥ 0 is obtained by writing $\mathcal{B}_{\text{LV}} = (\delta S_0 - \delta S_1)^2 - \sum_{i=1}^N [(s_0 - s_1)^2 - 2s_0^2 - 2s_1^2 + s_0 + s_1]^{(i)} \geq -\max_{s_0, s_1} E(s_0, s_1)$, where $E(s_0, s_1) = (s_0 - s_1)^2 - 2s_0^2 - 2s_1^2 + s_0 + s_1 = -(s_0 + s_1)(s_0 + s_1 - 1)$. Since $s_{0/1}$ are the outcomes of spin- j measurements, they are either both integers, either both half-integers. This implies that $s_0 + s_1$ is always an integer. Since $E(x) = -x(x-1) \leq 0$ for all integers x , we conclude that $\langle \mathcal{B} \rangle \geq 0$ for LV models. On the other hand, for the measurement setting we consider, we have the quantum value:

$$\langle \mathcal{B} \rangle = 4\text{Var}(\hat{J}_y) \sin^2 \theta - 2\langle \hat{J}_x \rangle \cos \theta + 4\cos^2 \theta \sum_{i=1}^N \langle [\hat{S}_x^{(i)}]^2 \rangle \quad (42)$$

We introduce the notation $s_x^2 = N^{-1} \sum_{i=1}^N \langle [\hat{S}_x^{(i)}]^2 \rangle$. The optimal measurement angle θ , leading to the minimal value of $\langle \mathcal{B} \rangle$, is s.t. $\cos \theta = \langle \hat{J}_x \rangle / [4Ns_x^2 - 4\text{Var}(\hat{J}_y)]$ (if this is ≤ 1), for which we obtain:

$$\langle \mathcal{B} \rangle = 4\text{Var}(\hat{J}_y) - \frac{\langle \hat{J}_x^2 \rangle}{4[Ns_x^2 - \text{Var}(\hat{J}_y)]}. \quad (43)$$

Violation is detected whenever $\langle \mathcal{B} \rangle < 0$. This generalizes the results for $j = 1/2$ [7, 19] to arbitrary spins. In Appendix B, we present another Bell's inequality, for which violation has been found with $j \leq 1$. Clearly,

adding extra measurements ($k \geq 3$) could only lead to more robust Bell's inequalities (see Sec. II D for the case $j = 1/2$): we leave this exploration open to future works.

IV. EXPERIMENTAL IMPLEMENTATION

Experimental detection of the Bell's inequalities discussed in this work require answering two questions:

- A) Can one detect the violation of the Bell's inequalities in question?
- B) Can one prepare the quantum many-body states that violate these Bell's inequalities?

The detection problem can take two conceptually-different forms: A1) the two-body correlations forming the Bell's inequalities are measured individually, which requires individual addressing of the subsystems; A2) only the witness inequalities, which involve fluctuations of collective variables, are measured. In the first case (A1), one realizes a situation conceptually close to a proper Bell test, even though avoiding e.g. the locality loophole might be very challenging. In contrast, in the second case (A2), one does not realize a Bell test, but rather demonstrates the ability to prepare many-body entangled states which would yield violation of the considered Bell's inequalities, if such a Bell test could be implemented. Clearly, violating the witness inequality is less demanding and requires only access to collective variables (as realized in [7, 12]), which are sums of spins or pseudo-spins of individual components of the system. These individual components could be atoms of spin $j = 1/2, 1, 3/2, \dots$, or atoms, ions and superconducting qubits realizing effective few-level systems. First- and second-moments of the collective-spin components must be measured.

Concerning the preparation, the goal is to generate strongly squeezed states or spin singlets, which appear as ground states of Hamiltonians with long-range interactions, such as, for instance, the ones corresponding to Lipkin-Meshkov-Glick models (see [20] and references therein). Notice that while spin singlets and spin squeezed states are paradigmatic examples of many-body entangled states, on which we focused in this work to demonstrate the effectiveness and flexibility of our new method, other classes of states are potentially interesting; for instance, Dicke states are clear candidates [21, 22] while the potentialities of $j \geq 1$ ensembles subjected to more general $SU(d)$ measurements, are virtually unlimited. In this section, we present an incomplete list of platforms for which both A and B questions can be answered positively.

Atomic ensembles. These are clouds of (not-necessarily cold) atoms with spin. A) The total spin components can be measured employing quantum Faraday effect, i.e.

looking at the polarisation rotation of the light passing through the atomic cloud [23]. This methods is also frequently termed as spin polarisation spectroscopy (SPS). In principle, one has access here to the full quantum statistics of the total spin components. Using standing driving fields, one can also detect spatial Fourier components of the collective spin [24]. B) Atomic ensembles are particularly suitable to achieve strong squeezing of the atomic spin. Using quantum feedback, spin singlet states have also been prepared [25–27]. Combining feedback with the ideas of Ref. [24], practically arbitrary spin-spin correlations could be generated [28]. Using a one-dimensional atom-light interface, quantum spin noise limit can be achieved [29]. Collective spin squeezed states and even Bell's non-locality can also be achieved for macroscopic ensembles using optical-cavity-assisted measurements [12].

Ultracold spinor Bose-Einstein condensates. A) The techniques developed for atomic ensembles can be applies to Bose-Einstein condensates [30]. In ultracold trapped spinor gases, the principal non-linear mechanism leading to squeezing (among other interesting entangled states) corresponds to spin-changing collisions [31]. Here, all spin components and their fluctuations can be measured. Beyond spin components, e.g. the nematic tensor for spin-1 condensates can be measured, including in a spatially-resolved way [32]. B) The possibility to violate the many-body Bell's inequalities of Ref. [6] were in fact first confirmed in twin-modes squeezed states in spinor condensates [7], and these systems allow one to generate non-classical states going beyond squeezing (for a review, see [18]). Entanglement between spatially separated condensates, and even Einstein-Podolsky-Rosen steering, can be generated [33, 34]. More recently, high-spin cold-atoms ensembles, which display dipolar magnetic interactions, have been generated [35–38], which appear as ideal playgrounds to explore Bell's inequalities tailored to arbitrary-spin systems, as established in the present work.

Ultracold atoms in optical lattices. A) Ultracold atoms in optical lattices provide one of the best platform for quantum simulations [39]. All the methods mentioned above can be carried over to atoms in optical lattices. SPS has emerged as a promising technique for detecting quantum phases in lattice gases via the coherent mapping of spin-correlations onto scattered light, realizing quantum non-demolition measurements. In particular, spatially-resolved SPS that employs standing wave laser configurations [24] allows for a direct probing of magnetic structure factors and order parameters [40–43]. Moreover, quantum gas microscopes, which are able to resolve individual atoms located in single lattice sites, have been developed [44–46]. These techniques allow for a direct inspection into the spatial structure of entanglement within the system [47], and direct violation of the Bell's inequalities (A1) could be envisioned. B)

In principle these systems may lead to a very large variety of strongly-correlated many-body states, and in particular spin singlets, which are ground states of quantum anti-ferromagnets, according to theorems by Mattis [48]. A review of potentially achievable correlations can be found in Ref. [49]. High-spin atomic ensembles in optical lattices [50, 51] clearly represent very promising systems to investigate novel classes of entangled many-body states, especially concerning Bell's inequalities involving many outcomes.

Trapped ions. A) Trapped ions represent a very versatile platform, and one of the most promising candidates for quantum computing. Small systems of ions allow for full quantum tomography of the density matrix, from which the statistics of all observables can be recovered. This includes in particular spin-spin correlations (see for instance [52]), but also e.g. third order correlations which have been used for the detection of genuine three-body entanglement in a system of few ions. Clearly, trapped ions are a platform of choice to directly probe the spatial structure of quantum correlations, and direct violation of the Bell's inequalities could be achieved (A1). B) Few-ion systems can be used for the generation of a very wide variety of entangled states on demand: recent examples include ground states of lattice gauge theory models, [53–55], and dynamically-generated entanglement [56], among others.

Significant others. These include, but are not limited to, atoms in nano-structures [57], Rydberg atoms [58], and a large number of condensed matter systems, ranging from circuit QED, through quantum dots, to superconducting Josephson junctions [59]. All of these systems could potentially prepare and detect the entangled states suitable to violate the Bell's inequalities investigated in this work – and, perhaps most importantly, generate correlation patterns from which data-driven methods such as ours could reveal other Bell's inequalities.

V. CONCLUSIONS

We have presented a new method for detecting multipartite entanglement in a device-independent scenario. Our convex-optimization algorithm (Section II A) constructs a violated Bell's inequality from one- and two-body correlations averaged over all permutations of the subsystems. Due to its very flexible nature, and a computational complexity which does not scale with the number of subsystems, this has allowed us to improve over existing many-body Bell's inequalities violated by $j = 1/2$ spin-squeezed and spin singlet states in the thermodynamic limit (Section II). In addition, we could extend these results to similar states for arbitrary $j > 1/2$ individual spins, by considering Bell scenarios with arbitrarily-many outcomes (Section III) – to our knowledge, this represents the first example of

such families of many-body Bell's inequalities. As our Bell's inequalities involve only zero-momentum fluctuations, sufficient conditions on many-body quantum states for their violation could be established, in the form of Bell-correlation witnesses. Such witnesses can be measured in state-of-the-art cold-atoms systems with only global measurements [7, 12] (Section IV). Due to its very flexible and intrinsically-scalable nature, our data-driven approach opens the way to the systematic exploration of permutationally-invariant Bell's inequalities in many-body quantum systems – as a matter of fact, the Bell's inequalities presented in the paper represent only a fraction of all those discovered with our approach [16], already for the simple classes of spin-squeezed and spin-singlet states. It would be interesting to explore other classes of many-body entangled states, e.g. Dicke states, and go beyond spin measurements to consider genuine $SU(d)$ measurement [32]. Finally, we would like to point out that, by construction, our algorithm searches for Bell's inequalities whose two-body coefficients form a positive semi-definite matrix. While all permutationally-invariant Bell's inequality which have been reported in the literature, and whose violation is robust in the thermodynamic limit, satisfy this condition, it would be interesting to understand its limitations.

Acknowledgments

We acknowledge the Spanish Ministry MINECO (National Plan 15 Grant: FISICATEAMO No. FIS2016-79508-P, SEVERO OCHOA No. SEV-2015-0522, FPI, FIS2020-TRANQI and Severo Ochoa CEX2019-000910-S), European Social Fund, Fundació Cellex, Fundació Mir-Puig, Generalitat de Catalunya (AGAUR Grant No. 2017 SGR 1341, AGAUR SGR 1381, CERCA program, QuantumCAT_U16-011424, co-funded by ERDF Operational Program of Catalonia 2014-2020), MINECO-EU QUANTERA MAQS (funded by The State Research Agency (AEI) PCI2019-111828-2 / 10.13039/501100011033), and the National Science Centre, Poland-Symfonia Grant No. 2016/20/W/ST4/00314. IF acknowledges support from the Mir-Puig and Cellex fundations through an ICFO-MPQ Postdoctoral Fellowship.

Appendix A: Convex optimization algorithm based on the averaged pair probability distribution

In this Section, we present a general formulation of the convex optimization algorithm to find a Bell's inequality violated by the pair probability distribution averaged over all permutations of the subsystems [Eq. (5)]:

$$\bar{P}(s, t|a, b) = \frac{1}{N(N-1)} \sum_{i \neq j} P^{(ij)}(s, t|a, b) . \quad (\text{A1})$$

The probability distribution \bar{P} is the central object reconstructed from experimental observations. $a, b = 0, \dots, k-1$ label the measurement settings, while $s, t = 1, \dots, d$ label the measurement outcomes. Assuming that a LV model $P_{\text{LV}}(\sigma)$ exists, which returns $P^{(ij)}$ as a marginal, with $\sigma = \{s_a^{(i)}\}$ a collection of classical variables representing the measurement outcomes, we have [Eq. (4)]:

$$P^{(ij)}(s, t|a, b) = \sum_{\sigma} P_{\text{LV}}(\sigma) \delta_{s_a^{(i)}, s} \delta_{s_b^{(j)}, t} . \quad (\text{A2})$$

We may then decompose \bar{P} as:

$$\bar{P} = \frac{1}{N(N-1)} \left[\sum_{i,j} P^{(ij)} - \sum_i P^{(ii)} \right] . \quad (\text{A3})$$

Even though $P^{(ii)}(s, t|a, b)$ is not observable (since it would require measuring simultaneously the settings a and b on the same subsystem i , and in general they correspond to incompatible quantum observables), it exists at the level of the LV model. The key point is then that if we define $Q_{(s,a),(t,b)} = \sum_{i,j} P^{(ij)}(s, t|a, b)$, then Q [as a $(kd) \times (kd)$ matrix] is PSD. Indeed, considering a kd -component vector $f(s|a)$, we have:

$$\begin{aligned} f^T Q f &= \sum_{s,t} \sum_{a,b} \sum_{i,j} P^{(ij)}(s, t|a, b) f(s|a) f(t|b) \\ &= \sum_{\sigma} P_{\text{LV}}(\sigma) \sum_{i,j} \sum_{a,b} \sum_{s,t} \delta_{s_a^{(i)}, s} f(s|a) \delta_{s_b^{(j)}, t} f(t|b) \\ &= \sum_{\sigma} P_{\text{LV}}(\sigma) \sum_{i,j} \sum_{a,b} f[s_a^{(i)}|a] f[s_b^{(j)}|b] \\ &= \sum_{\sigma} P_{\text{LV}}(\sigma) \left\{ \sum_i \sum_a f[s_a^{(i)}|a] \right\}^2 \\ &\geq 0 . \end{aligned} \quad (\text{A4})$$

Consequently, for any PSD matrix $M_{(s,a),(t,b)} := M(s, t|a, b)$, we have:

$$\begin{aligned} \sum_{a,b} \sum_{s,t} M(s, t|a, b) \bar{P}(s, t|a, b) &\geq \\ -\frac{1}{N(N-1)} \sum_i \sum_{a,b} \sum_{s,t} M(s, t|a, b) P^{(ii)}(s, t|a, b) &\geq -\frac{1}{N-1} E_{\text{max}}(M) , \end{aligned} \quad (\text{A5})$$

where:

$$E_{\text{max}}(M) = \max_{s \in \{1, \dots, d\}^k} \sum_{a,b} M(s_a, s_b|a, b) . \quad (\text{A6})$$

The optimal PSD matrix M may therefore be found by a convex-optimization program, minimizing the cost function:

$$L(M) = \sum_{a,b} \sum_{s,t} M(s, t|a, b) \bar{P}(s, t|a, b) + \frac{1}{N-1} E_{\text{max}}(M) \quad (\text{A7})$$

over all PSD matrices M .

Appendix B: Bell's inequality for spin-squeezed states

Exploring $j = 1$ spin-squeezed states with $k = 2$ spin measurements in the xy -plane, at angle $\pm\theta$ with respect to the x axis, we found another violated Bell's inequality similar to the one presented in Section II D:

$$\langle \mathcal{B} \rangle = \tilde{C}_{00} + \tilde{C}_{11} - \tilde{C}_{01} - \tilde{C}_{10} + M_0^{(2)} + M_1^{(2)} - 2M_0 - 2M_1 \quad (\text{B1})$$

$$= \langle \delta(S_0 - S_1)^2 \rangle + 2 \sum_{i=1}^N \langle s_0 s_1 - s_0 - s_1 \rangle^{(i)} \quad (\text{B2})$$

$$\geq -2Nj^2 . \quad (\text{B3})$$

The quantum value is (with $s_a^2 = N^{-1} \sum_{i=1}^N \langle [\hat{S}_a^{(i)}]^2 \rangle$ for $a = x, y$):

$$\langle \mathcal{B} \rangle = 4\text{Var}(\hat{J}_y) \sin^2 \theta - 4\langle \hat{J}_x \rangle \cos \theta + 2N(s_x^2 \cos^2 \theta - s_y^2 \sin^2 \theta) \quad (\text{B4})$$

The optimal angle is s.t. $\cos \theta = \langle \hat{J}_x \rangle / [Ns_x^2 + Ns_y^2 - 2\text{Var}(\hat{J}_y)]$, for which we have:

$$\langle \mathcal{B} \rangle = 2[2\text{Var}(\hat{J}_y) - Ns_y^2] - \frac{2\langle \hat{J}_x \rangle^2}{Ns_x^2 + Ns_y^2 - 2\text{Var}(\hat{J}_y)} \quad (\text{B5})$$

We found violation for squeezed states of $j = 1/2$ or $j = 1$.

[1] Georgescu, I. M., Ashhab, S. & Nori, F. Quantum simulation. *Rev. Mod. Phys.* **86**, 153–185 (2014). URL <https://link.aps.org/doi/10.1103/RevModPhys.86.153>.

[2] Deutsch, I. H. Harnessing the power of the second quantum revolution. *PRX Quantum* **1**, 020101 (2020). URL <https://link.aps.org/doi/10.1103/PRXQuantum.1.020101>.

[3] Gühne, O. & Tóth, G. Entanglement detection. *Physics Reports* **474**, 1–75 (2009). URL <http://www.sciencedirect.com/science/article/pii/S0370157309000623>.

[4] Brunner, N., Cavalcanti, D., Pironio, S., Scarani, V. & Wehner, S. Bell nonlocality. *Rev. Mod. Phys.* **86**, 419–478 (2014). URL <https://link.aps.org/doi/10.1103/RevModPhys.86.419>.

[5] Paris, M. & Rehacek, J. *Quantum State Estimation*. Lecture Notes in Physics (Springer Berlin Heidelberg, 2004). URL <https://www.springer.com/gp/book/9783540223290>.

[6] Tura, J. *et al.* Detecting nonlocality in many-body quan-

tum states. *Science* **344**, 1256–1258 (2014). URL <http://science.sciencemag.org/content/344/6189/1256>.

[7] Schmied, R. *et al.* Bell correlations in a Bose-Einstein condensate. *Science* **352**, 441–444 (2016). URL <http://science.sciencemag.org/content/352/6284/441>.

[8] Baccari, F., Cavalcanti, D., Wittek, P. & Acín, A. Efficient device-independent entanglement detection for multipartite systems. *Phys. Rev. X* **7**, 021042 (2017). URL <https://link.aps.org/doi/10.1103/PhysRevX.7.021042>.

[9] Frérot, I. & Roscilde, T. Detecting many-body bell nonlocality by solving ising models (2020). URL <https://arxiv.org/abs/2004.07796>. 2004.07796.

[10] Tóth, G., Knapp, C., Gühne, O. & Briegel, H. J. Spin squeezing and entanglement. *Phys. Rev. A* **79**, 042334 (2009). URL <https://link.aps.org/doi/10.1103/PhysRevA.79.042334>.

[11] Fadel, M. & Tura, J. Bounding the set of classical correlations of a many-body system. *Phys. Rev. Lett.* **119**, 230402 (2017). URL <https://link.aps.org/doi/10.1103/PhysRevLett.119.230402>.

[12] Engelsen, N. J., Krishnakumar, R., Hosten, O. & Kasevich, M. A. Bell Correlations in Spin-Squeezed States of 500 000 Atoms. *Phys. Rev. Lett.* **118**, 140401 (2017). URL <https://link.aps.org/doi/10.1103/PhysRevLett.118.140401>.

[13] Wang, Z., Singh, S. & Navascués, M. Entanglement and nonlocality in infinite 1d systems. *Phys. Rev. Lett.* **118**, 230401 (2017). URL <https://link.aps.org/doi/10.1103/PhysRevLett.118.230401>.

[14] Bell, J. S. On the Einstein Podolski Rosen paradox. *Physics* **1**, 195–200 (1964).

[15] Fine, A. Hidden variables, joint probability, and the bell inequalities. *Phys. Rev. Lett.* **48**, 291–295 (1982). URL <https://link.aps.org/doi/10.1103/PhysRevLett.48.291>.

[16] A pedagogical version of the code used to discover the Bell's inequalities of the paper and generate the figures is available at the following address. URL https://github.com/GuillemMRR/Many-body_Bells_inequalities_from_averaged_two-body_correlations.

[17] Boyd, S., Boyd, S., Vandenberghe, L. & Press, C. U. *Convex Optimization* (Cambridge University Press, 2004).

[18] Pezzè, L., Smerzi, A., Oberthaler, M. K., Schmied, R. & Treutlein, P. Quantum metrology with nonclassical states of atomic ensembles. *Reviews of Modern Physics* **90**, 035005 (2018). URL <https://link.aps.org/doi/10.1103/RevModPhys.90.035005>.

[19] Piga, A., Aloy, A., Lewenstein, M. & Frérot, I. Bell Correlations at Ising Quantum Critical Points. *Phys. Rev. Lett.* **123**, 170604 (2019). URL <https://link.aps.org/doi/10.1103/PhysRevLett.123.170604>.

[20] Bao, J., Guo, B., Liu, Y.-H., Shen, L.-H. & Sun, Z.-Y. Multipartite nonlocality and global quantum discord in the antiferromagnetic lipkin–meshkov–glick model. *Physica B: Condensed Matter* **593**, 412297 (2020). URL <http://www.sciencedirect.com/science/article/pii/S0921452620303112>.

[21] Lücke, B. *et al.* Twin matter waves for interferometry beyond the classical limit. *Science* **334**, 773–776 (2011). URL <https://science.sciencemag.org/content/334/6057/773>. <https://science.sciencemag.org/content/334/6057/773.full.pdf>.

[22] Zou, Y.-Q. *et al.* Beating the classical pre-
cision limit with spin-1 dicke states of more than 10,000 atoms. *Proceedings of the National Academy of Sciences* **115**, 6381–6385 (2018). URL <https://www.pnas.org/content/115/25/6381>. <https://www.pnas.org/content/115/25/6381.full.pdf>.

[23] Hammerer, K., Sørensen, A. S. & Polzik, E. S. Quantum interface between light and atomic ensembles. *Rev. Mod. Phys.* **82**, 1041–1093 (2010). URL <https://link.aps.org/doi/10.1103/RevModPhys.82.1041>.

[24] Eckert, K. *et al.* Quantum non-demolition detection of strongly correlated systems. *Nature Physics* **4**, 50–54 (2008). URL <http://www.nature.com/articles/nphys776>. Number: 1 Publisher: Nature Publishing Group.

[25] Tóth, G. & Mitchell, M. W. Generation of macroscopic singlet states in atomic ensembles. *New Journal of Physics* **12**, 053007 (2010). URL <https://doi.org/10.1088/21367-2630%2F12%2F5%2F053007>. Publisher: IOP Publishing.

[26] Urizar-Lanz, I., Hyllus, P., Egusquiza, I. L., Mitchell, M. W. & Tóth, G. Macroscopic singlet states for gradient magnetometry. *Physical Review A* **88**, 013626 (2013). URL <https://link.aps.org/doi/10.1103/PhysRevA.88.013626>. Publisher: American Physical Society.

[27] Behbood, N. *et al.* Generation of Macroscopic Singlet States in a Cold Atomic Ensemble. *Physical Review Letters* **113**, 093601 (2014). URL <https://link.aps.org/doi/10.1103/PhysRevLett.113.093601>. Publisher: American Physical Society.

[28] Hauke, P., Sewell, R. J., Mitchell, M. W. & Lewenstein, M. Quantum control of spin correlations in ultracold lattice gases. *Physical Review A* **87**, 021601 (2013). URL <https://link.aps.org/doi/10.1103/PhysRevA.87.021601>. Publisher: American Physical Society.

[29] Béguin, J.-B., Müller, J., Appel, J. & Polzik, E. Observation of Quantum Spin Noise in a 1D Light-Atoms Quantum Interface. *Physical Review X* **8**, 031010 (2018). URL <https://link.aps.org/doi/10.1103/PhysRevX.8.031010>. Publisher: American Physical Society.

[30] Eckert, K., Zawitkowski, L., Sanpera, A., Lewenstein, M. & Polzik, E. S. Quantum Polarization Spectroscopy of Ultracold Spinor Gases. *Physical Review Letters* **98**, 100404 (2007). URL <https://link.aps.org/doi/10.1103/PhysRevLett.98.100404>. Publisher: American Physical Society.

[31] Schmaljohann, H. *et al.* Dynamics of \$F=2\$ Spinor Bose-Einstein Condensates. *Physical Review Letters* **92**, 040402 (2004). URL <https://link.aps.org/doi/10.1103/PhysRevLett.92.040402>. Publisher: American Physical Society.

[32] Kunkel, P. *et al.* Simultaneous readout of noncommuting collective spin observables beyond the standard quantum limit. *Phys. Rev. Lett.* **123**, 063603 (2019). URL <https://link.aps.org/doi/10.1103/PhysRevLett.123.063603>.

[33] Fadel, M., Zibold, T., Décamps, B. & Treutlein, P. Spatial entanglement patterns and Einstein-Podolsky-Rosen steering in Bose-Einstein condensates. *Science* **360**, 409–413 (2018). URL <http://science.sciencemag.org/content/360/6387/409>. Publisher: American Association for the Advancement of Science Section: Report.

[34] Lange, K. *et al.* Entanglement between two spatially separated atomic modes. *Science* **360**, 416–418 (2018). URL <http://science.sciencemag.org/content/360/6387/416>. Publisher: American Association for the Advancement of Science Section: Report.

[35] Bataille, P. *et al.* Adiabatic spin-dependent momentum transfer in an $su(n)$ degenerate fermi gas. *Phys. Rev. A* **102**, 013317 (2020). URL <https://link.aps.org/doi/10.1103/PhysRevA.102.013317>.

[36] Trautmann, A. *et al.* Dipolar quantum mixtures of erbium and dysprosium atoms. *Phys. Rev. Lett.* **121**, 213601 (2018). URL <https://link.aps.org/doi/10.1103/PhysRevLett.121.213601>.

[37] Tanzi, L. *et al.* Supersolid symmetry breaking from compressional oscillations in a dipolar quantum gas. *Nature* **574**, 382–385 (2019). URL <http://www.nature.com/articles/s41586-019-1568-6>. Number: 7778 Publisher: Nature Publishing Group.

[38] Böttcher, F. *et al.* New states of matter with fine-tuned interactions: quantum droplets and dipolar supersolids. *arXiv e-prints* arXiv:2007.06391 (2020). 2007.06391.

[39] Lewenstein, M., Sanpera, A. & Ahufinger, V. *Ultracold Atoms in Optical Lattices: Simulating quantum many-body systems* (OUP Oxford, 2012). Google-Books-ID: Wpl91RDxV5IC.

[40] Roscilde, T. *et al.* Quantum polarization spectroscopy of correlations in attractive fermionic gases. *New Journal of Physics* **11**, 055041 (2009). URL <http://iopscience.iop.org/article/10.1088/1367-2630/11/5/055041/meta>. Publisher: IOP Publishing.

[41] De Chiara, G., Romero-Isart, O. & Sanpera, A. Probing magnetic order in ultracold lattice gases. *Physical Review A* **83**, 021604 (2011). URL <https://link.aps.org/doi/10.1103/PhysRevA.83.021604>. Publisher: American Physical Society.

[42] Weitenberg, C. *et al.* Coherent Light Scattering from a Two-Dimensional Mott Insulator. *Physical Review Letters* **106**, 215301 (2011). URL <https://link.aps.org/doi/10.1103/PhysRevLett.106.215301>. Publisher: American Physical Society.

[43] Meineke, J. *et al.* Interferometric measurement of local spin fluctuations in a quantum gas. *Nature Physics* **8**, 454–458 (2012). URL <http://www.nature.com/articles/nphys2280>. Number: 6 Publisher: Nature Publishing Group.

[44] Bakr, W. S., Gillen, J. I., Peng, A., Fölling, S. & Greiner, M. A quantum gas microscope for detecting single atoms in a Hubbard-regime optical lattice. *Nature* **462**, 74–77 (2009). URL <http://www.nature.com/articles/nature08482>. Number: 7269 Publisher: Nature Publishing Group.

[45] Sherson, J. F. *et al.* Single-atom-resolved fluorescence imaging of an atomic Mott insulator. *Nature* **467**, 68–72 (2010). URL <http://www.nature.com/articles/nature09378>. Number: 7311 Publisher: Nature Publishing Group.

[46] Ott, H. Single atom detection in ultracold quantum gases: a review of current progress. *Reports on Progress in Physics* **79**, 054401 (2016). URL <https://doi.org/10.1088%2F0034-4885%2F79%2F5%2F054401>. Publisher: IOP Publishing.

[47] Fukuhara, T. *et al.* Spatially resolved detection of a spin-entanglement wave in a bose-hubbard chain. *Phys. Rev. Lett.* **115**, 035302 (2015). URL <https://link.aps.org/doi/10.1103/PhysRevLett.115.035302>.

[48] Auerbach, A. *Interacting Electrons and Quantum Magnetism*. Graduate Texts in Contemporary Physics (Springer-Verlag, New York, 1994). URL <https://www.springer.com/gp/book/9780387942865>.

[49] De Chiara, G. & Sanpera, A. Genuine quantum correlations in quantum many-body systems: a review of recent progress. *arXiv:1711.07824 [cond-mat, physics:quant-ph]* (2018). URL <http://arxiv.org/abs/1711.07824>. ArXiv: 1711.07824.

[50] Gabardos, L. *et al.* Relaxation of the collective magnetization of a dense 3d array of interacting dipolar $s = 3$ atoms. *Phys. Rev. Lett.* **125**, 143401 (2020). URL <https://link.aps.org/doi/10.1103/PhysRevLett.125.143401>.

[51] Patscheider, A. *et al.* Controlling dipolar exchange interactions in a dense three-dimensional array of large-spin fermions. *Phys. Rev. Research* **2**, 023050 (2020). URL <https://link.aps.org/doi/10.1103/PhysRevResearch.2.023050>.

[52] Brydges, T. *et al.* Probing rényi entanglement entropy via randomized measurements. *Science* **364**, 260–263 (2019). URL <https://science.sciencemag.org/content/364/6437/260>. <https://science.sciencemag.org/content/364/6437/260.full.pdf>.

[53] Kokail, C. *et al.* Self-verifying variational quantum simulation of lattice models. *Nature* **569**, 355–360 (2019). URL <http://www.nature.com/articles/s41586-019-1177-4>. Number: 7756 Publisher: Nature Publishing Group.

[54] Bañuls, M. C. *et al.* Simulating Lattice Gauge Theories within Quantum Technologies. *The European Physical Journal D* **74**, 165 (2020). URL <http://arxiv.org/abs/1911.00003>. ArXiv: 1911.00003.

[55] Martinez, E. A. *et al.* Real-time dynamics of lattice gauge theories with a few-qubit quantum computer. *Nature* **534**, 516–519 (2016). URL <http://www.nature.com/articles/nature18318>. Number: 7608 Publisher: Nature Publishing Group.

[56] Zhang, J. *et al.* Observation of a many-body dynamical phase transition with a 53-qubit quantum simulator. *Nature* **551**, 601–604 (2017). URL <http://www.nature.com/articles/nature24654>. Number: 7682 Publisher: Nature Publishing Group.

[57] Chang, D. E., Cirac, J. I. & Kimble, H. J. Self-Organization of Atoms along a Nanophotonic Waveguide. *Physical Review Letters* **110**, 113606 (2013). URL <https://link.aps.org/doi/10.1103/PhysRevLett.110.113606>. Publisher: American Physical Society.

[58] Bernien, H. *et al.* Probing many-body dynamics on a 51-atom quantum simulator. *Nature* **551**, 579–584 (2017). URL <http://www.nature.com/articles/nature24622>. Number: 7682 Publisher: Nature Publishing Group.

[59] Arute, F. *et al.* Quantum supremacy using a programmable superconducting processor. *Nature* **574**, 505–510 (2019). URL <http://www.nature.com/articles/s41586-019-1666-5>. Number: 7779 Publisher: Nature Publishing Group.